PHYSICAL REVIEW B **89**, 220508(R) (2014)

Coexistence of Bloch electrons and glassy electrons in $Ca_{10}(Ir_4As_8)(Fe_{2-x}Ir_xAs_2)_5$ revealed by angle-resolved photoemission spectroscopy

K. Sawada,[1] D. Ootsuki,[1] K. Kudo,[2] D. Mitsuoka,[2] M. Nohara,[2] T. Noda,[1] K. Horiba,[3] M. Kobayashi,[3] K. Ono,[3] H. Kumigashira,[3] N. L. Saini,[4] and T. Mizokawa[1,4]

[1]*Department of Complexity Science and Engineering and Department of Physics, University of Tokyo, 5-1-5 Kashiwanoha, Chiba 277-8561, Japan*

[2]*Department of Physics, Okayama University, Kita-ku, Okayama 700-8530, Japan*

[3]*Institute of Materials Structure Science, High Energy Accelerator Research Organization (KEK), Tsukuba, Ibaraki 305-0801, Japan*

[4]*Department of Physics, University of Roma "La Sapienza" Piazalle Aldo Moro 2, 00185 Roma, Italy*

(Received 21 May 2014; revised manuscript received 12 June 2014; published 25 June 2014)

Angle-resolved photoemission spectroscopy of $Ca_{10}(Ir_4As_8)(Fe_{2-x}Ir_xAs_2)_5$ shows that the Fe 3*d* electrons in the FeAs layer form the holelike Fermi pocket at the zone center and the electronlike Fermi pockets at the zone corners as commonly seen in various Fe-based superconductors. The FeAs layer is heavily electron doped and has relatively good two dimensionality. On the other hand, the Ir 5*d* electrons are metallic and glassy probably due to atomic disorder related to the Ir 5*d* orbital instability. $Ca_{10}(Ir_4As_8)(Fe_{2-x}Ir_xAs_2)_5$ exhibits a unique electronic state where the Bloch electrons in the FeAs layer coexist with the glassy electrons in the Ir_4As_8 layer.

DOI: 10.1103/PhysRevB.89.220508 PACS number(s): 74.25.Jb, 74.70.Dd, 79.60.−i

The discoveries of the superconductivity in the layered LaOFeP [1] and LaOFeAs [2] systems have induced intensive research activity on the physical properties of Fe pnictides. The Fe pnictide superconductors commonly have the FeAs layers, where each Fe ion is tetrahedrally coordinated by four pnictogen ions and the Fe ions form a square lattice. In most of the Fe pnictide superconductors, the FeAs layer has the holelike Fermi pocket at the zone center and the electronlike Fermi pockets at the zone corners which have been observed by angle-resolved photoemission spectroscopy (ARPES) in the early stage [3–7]. The FeAs layers are separated by the spacer layers such as LaO, and modifications of the spacer layers often play essential roles in control of the superconducting properties and the electronic structures of the FeAs layers. Recently, $Ca_{10}(Pt_4As_8)(Fe_{2-x}Pt_xAs_2)_5$ with Pt_4As_8 spacer layer has been discovered [8–11] and has been attracting great interest due to a possible interplay between the Pt_4As_8 layer and the FeAs layer. $Ca_{10}(Pt_4As_8)(Fe_{2-x}Pt_xAs_2)_5$ exhibits superconductivity at 38 K and the Pt_4As_8 spacer layer is considered to provide electrons to the superconducting FeAs layer. The Pt_4As_8 spacer layer consists of $PtAs_4$ square-planar geometry and is predicted to be metallic. Namely, the Pt 5*d* orbitals hybridize with the Fe 3*d* states at the Fermi level (E_F). However, such hybridization between the Pt 5*d* and Fe 3*d* orbitals at E_F is not clearly observed by ARPES, indicating that the Pt_4As_8 spacer layer is semiconducting [12,13]. On the other hand, another recent ARPES study has shown that the Pt 5*d* states have small contribution to the Fermi surfaces, partly consistent with the theoretical prediction [14]. In the case of $Ca_{10}(Pt_4As_8)(Fe_{2-x}Pt_xAs_2)_5$, the contribution of the Pt 5*d* states at E_F is rather small even though it may exist as predicted by the theory.

Isostructural $Ca_{10}(Ir_4As_8)(Fe_{2-x}Ir_xAs_2)_5$ is another member of the iron-based superconductors with $T_c = 16$ K [15]. This material has square-planar Ir_4As_8 layers, which are isotypic to the Pt_4As_8 layers in $Ca_{10}(Pt_4As_8)(Fe_{2-x}Pt_xAs_2)_5$. The band-structure calculation for $Ca_{10}(Ir_4As_8)(Fe_{2-x}Ir_xAs_2)_5$ predicts that the Ir 5*d* orbitals have relatively large contribution to the density of states at E_F compared to $Ca_{10}(Pt_4As_8)(Fe_{2-x}Pt_xAs_2)_5$ [15]. In addition, a recent x-ray-diffraction study by Sugawara *et al.* has reported doubling of the unit cell along the *c* axis below 100 K, which is attributed to the Ir 5*d* orbital instability [16]. In this context, an ARPES study on $Ca_{10}(Ir_4As_8)(Fe_{2-x}Ir_xAs_2)_5$ is highly interesting and important in order to reveal the electronic structure of the Ir_4As_8 layer as well as its impact on the FeAs layer. In this work, on the basis of photoemission spectroscopy, we discuss the unusual electronic structure of $Ca_{10}(Ir_4As_8)(Fe_{2-x}Ir_xAs_2)_5$ where Bloch-like Fe 3*d* electrons forming the hole and electron Fermi pockets coexist with metallic and glassy Ir 5*d* electrons.

The single crystal samples of $Ca_{10}(Ir_4As_8)(Fe_{2-x}Ir_xAs_2)_5$ were prepared as reported in the literature [15]. The lattice constants *a* and *c* are ∼8.725 Å and 20.70 Å around 20 K [16]. The ARPES measurements were performed at beamline 28A of Photon Factory, KEK using a SCIENTA SES-2002 electron analyzer with circularly polarized light. We have employed circularly polarized light in order to avoid the relatively strict selection rule of the linear polarization and to observe various Fe 3*d* and Ir 5*d* orbital symmetries. The total energy resolution was set to 20–30 meV for the excitation energies from $h\nu = 37$ eV to 67 eV. The angular resolution was set to ∼0.2°, which gives the momentum resolution of 0.01–0.015 $Å^{-1}$ for $h\nu = 37$–67 eV. The base pressure of the spectrometer was in the 10^{-9} Pa range. The single crystals of $Ca_{10}(Ir_4As_8)(Fe_{2-x}Ir_xAs_2)_5$, oriented by *ex situ* Laue diffraction, were cleaved at 20 K under the ultrahigh vacuum and the spectra were acquired at 20 K within 12 h after the cleaving. E_F was determined using the Fermi edge of gold reference samples.

The valence-band photoemission spectra of $Ca_{10}(Ir_4As_8)(Fe_{2-x}Ir_xAs_2)_5$ taken at photon energies from $h\nu = 55$ eV to 67 eV are displayed in Fig. 1. The peak near E_F dramatically gains its intensity in going from $h\nu = 55$ eV to 67 eV, consistent with the Fe 3*p*-3*d* resonance behavior observed in $LaFeAsO_{1-x}F_x$ [17]. In contrast, the intensity of the region from 2 to 4 eV below E_F does not depend appreciably on the photon energy. The photon energy dependence of the valence-band spectra is basically consistent

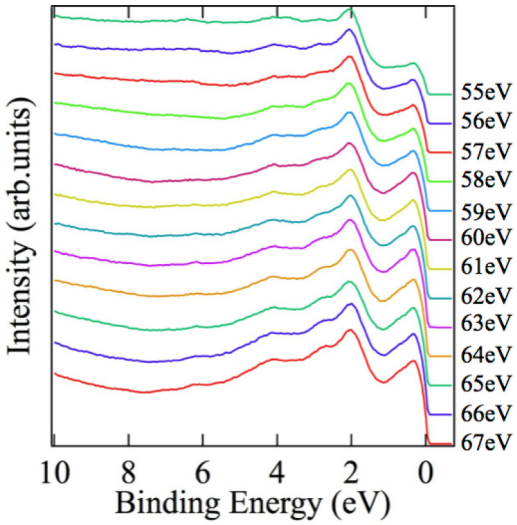

FIG. 1. (Color online) Valence-band photoemission spectra of $Ca_{10}(Ir_4As_8)(Fe_{2-x}Ir_xAs_2)_5$ taken at $h\nu = 55$–67 eV.

with the density of states calculated by Kudo *et al.* [15]. The calculation indicates that the structure near E_F is dominated by the Fe $3d$ orbitals with a mixture of the broad Ir $5d$ e_g band, consistent with the Fe $3p$-$3d$ resonance behavior. On the other hand, due to the weak resonance behavior, the structure ranging from 2 to 4 eV below E_F can be assigned to the relatively narrow Ir $5d$ t_{2g} band which is mixed with the Fe $3d$ orbitals and is located around 2–4 eV below E_F in the calculation. The overall agreement with the band-structure calculation suggests that the Ir $5d$ e_g electrons contribute to the density states at E_F as predicted by the calculation.

Figures 2(a)–2(c) show the Fermi surface maps taken at $h\nu = 41$, 45, and 50 eV. In the Fermi surface maps, the ARPES intensity $\rho(E)$ is integrated within energy window $|E - E_F| < 5$ meV and is displayed as a function of k_x and k_y. Here, k_x (or k_y) is the electron momentum approximately along the Fe-Fe direction of the FeAs layer, and the two-dimensional Brillouin zone for the FeAs layer is indicated by the solid lines in Figs. 2(a)–2(c). The holelike Fermi pocket at the zone center and the four electronlike Fermi pockets at the zone corners are observed by ARPES as commonly seen in various Fe-based superconductors. The four electron pockets are schematically shown by the four ellipses. Here, it should be noted that the periodicity of the observed electron pockets is not clear in the maps and that the estimated positions of the four corners of the square Brillouin zone have uncertainty. However, in spite of the uncertainty, one can safely conclude that the holelike and electronlike Fermi pockets are derived from the FeAs layer. The Fermi surface maps of Figs. 2(a)–2(c) are taken at $h\nu = 41$, 45, and 50 eV, which correspond to k_z (momentum perpendicular to the FeAs layer or the Ir_4As_8 layer) of 3.64 Å^{-1} ($\sim 12 \times 2\pi/c$), 3.78 Å^{-1} ($\sim 12.5 \times 2\pi/c$), and 3.95 Å^{-1} ($\sim 13 \times 2\pi/c$) at the zone center ($k_x = k_y = 0$), respectively. Whereas the area of the holelike Fermi pocket at the zone center is very small, those of the electronlike Fermi pockets at the zone corners are relatively large for all the k_z values, indicating that the FeAs layer is heavily electron doped. On the other hand, the Fermi surfaces from the Ir_4As_8 layer

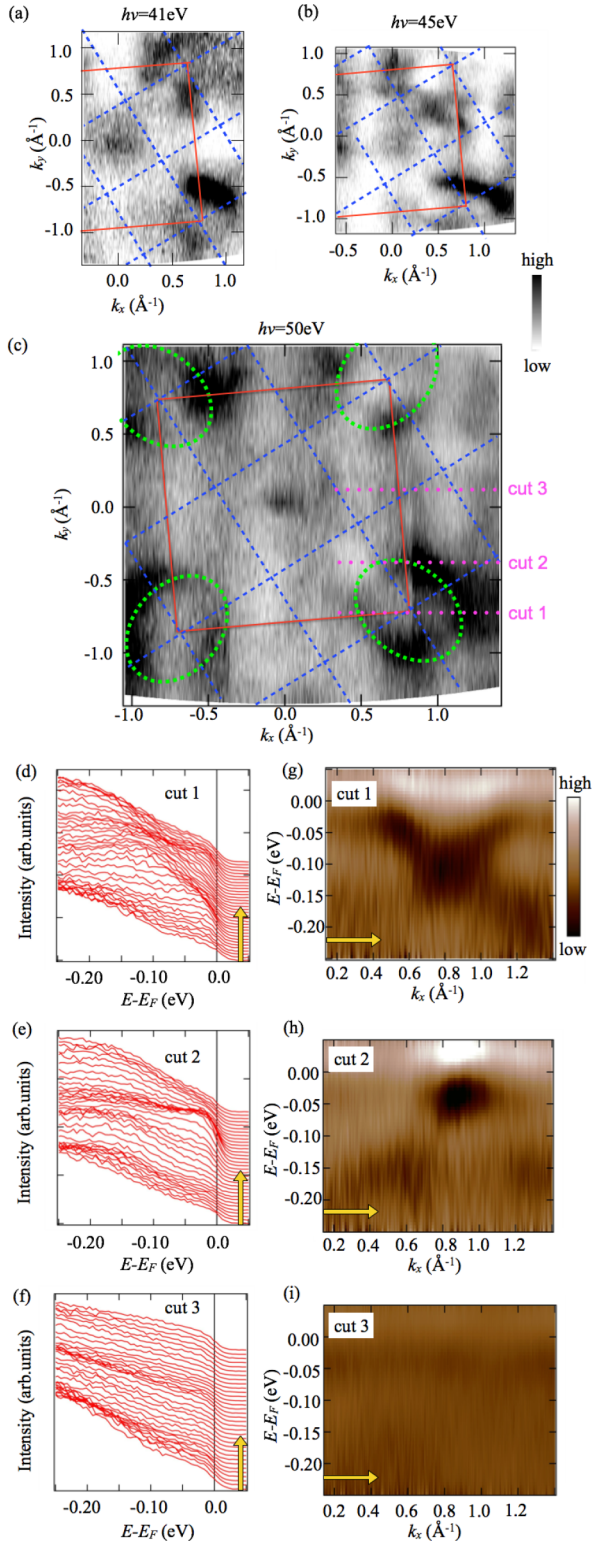

FIG. 2. (Color online) Fermi surface maps (a) taken at $h\nu = 41.0$ eV, (b) taken at $h\nu = 45.0$ eV, and (c) taken at $h\nu = 50.0$ eV. Two-dimensional Brillouin zones for the FeAs layer and the Ir_4As_8 layer are indicated by the red solid lines and by the blue dotted lines, respectively. The electronlike Fermi pockets of the FeAs layer are indicated by the dotted ellipses around the zone corners. Energy distribution curves (d) along cut 1, (e) along cut 2, and (f) along cut 3 in the Fermi surface map at $h\nu = 50.0$ eV. Second derivative plots (g) along cut 1, (h) along cut 2, and (i) along cut 3.

are apparently absent, which may contradict the theoretical prediction of the metallic Ir_4As_8 layer.

Figures 2(d)–2(f) show the ARPES intensity or the energy distribution curves $\rho(E)$ along cuts 1, 2, and 3 in the Fermi surface map of Fig. 2(c), respectively. In Figs. 2(g)–2(i), the second derivatives $d^2\rho(E)/dE^2$ are plotted as functions of the momentum along cuts 1, 2, and 3. The low value of $d^2\rho(E)/dE^2$ corresponds to the peak in $\rho(E)$. First, dispersion of the electronlike band is clearly seen along cut 1 in Figs. 2(d) as well as in the second derivative plot in Fig. 2(g). The electron-like Fermi pocket is still observed along cut 2 showing that the area of the electronlike Fermi pockets is substantially large as schematically indicated by the dotted ellipse in Fig. 2(c). The bottom of the electron band at the zone corner is located around 0.1 eV below E_F, which is very far from E_F compared to those of the various Fe-based superconductors. For example, the bottom of the electron band at zone corner is located around 0.03 eV below E_F in optimally electron-doped $Ba(Fe_{1-x}Co_x)_2As_2$ with $x = 0.06$ and around 0.1 eV below E_F in heavily electron-doped $Ba(Fe_{1-x}Co_x)_2As_2$ with $x = 0.24$ [18]. This observation is again consistent with the heavy electron doping in the FeAs layer and with the estimation by Kudo *et al.* [15]. Secondly, even outside of the electronlike Fermi pockets, substantial spectral weight at E_F is observed. As shown in Fig. 2(f), the spectral weight at E_F is seen even along cut 3 where no Fermi surface is expected and is observed indeed [also see the second derivative plot in Fig. 2(i)]. The momentum-independent spectral weight at E_F indicates glassy (and metallic) electronic states which may be induced by atomic disorder. Since the electronlike and holelike Fermi pockets are derived from the FeAs layer, the glassy spectral weight can be attributed to the Ir_4As_8 layer which may be atomically disordered by the Ir $5d$ e_g orbital instability. This picture is indeed consistent with the extended x-ray absorption fine structure at the Ir L edge [19]. Such glassy spectral weight at E_F is specific to $Ca_{10}(Ir_4As_8)(Fe_{2-x}Ir_xAs_2)_5$ and does not exist in $Ca_{10}(Pt_4As_8)(Fe_{2-x}Pt_xAs_2)_5$ [12–14,20].

Figure 3(a) shows a Fermi surface map in the k_x-k_z plane. The holelike Fermi pocket around the zone center is clearly seen in the wide k_z region, and the k_z dependence of the Fermi pocket is rather small. This indicates that two dimensionality of the Fe $3d$ bands is relatively good in the present system and would be inconsistent with the metallic Ir_4As_8 layer since the metallic spacer layer is expected to provide strong interlayer interaction. However, if the metallic Ir_4As_8 layer is strongly disordered as discussed in the previous paragraph, the interlayer interaction becomes momentum independent and, consequently, the FeAs layer can exhibit good two dimensionality although the Ir_4As_8 interlayer is metallic.

Figures 3(b)–3(f) show energy distribution curves taken at $h\nu = 60$, 54, 50, 45, and 41 eV. In addition to the holelike Fermi pocket at the zone center, the momentum-independent spectral weight is seen at E_F. This is again consistent with the picture that the momentum-dependent Fermi pocket is derived from the FeAs layer and that the momentum-independent states are assigned to the atomically disordered Ir_4As_8 layer. The band dispersion of the hole band is seen in the second derivative plots of Figs. 3(g)–3(k). Only one hole band is observed although three hole bands (one Fe $3d$ xy band and two Fe $3d$ yz/zx bands) are expected from the theoretical

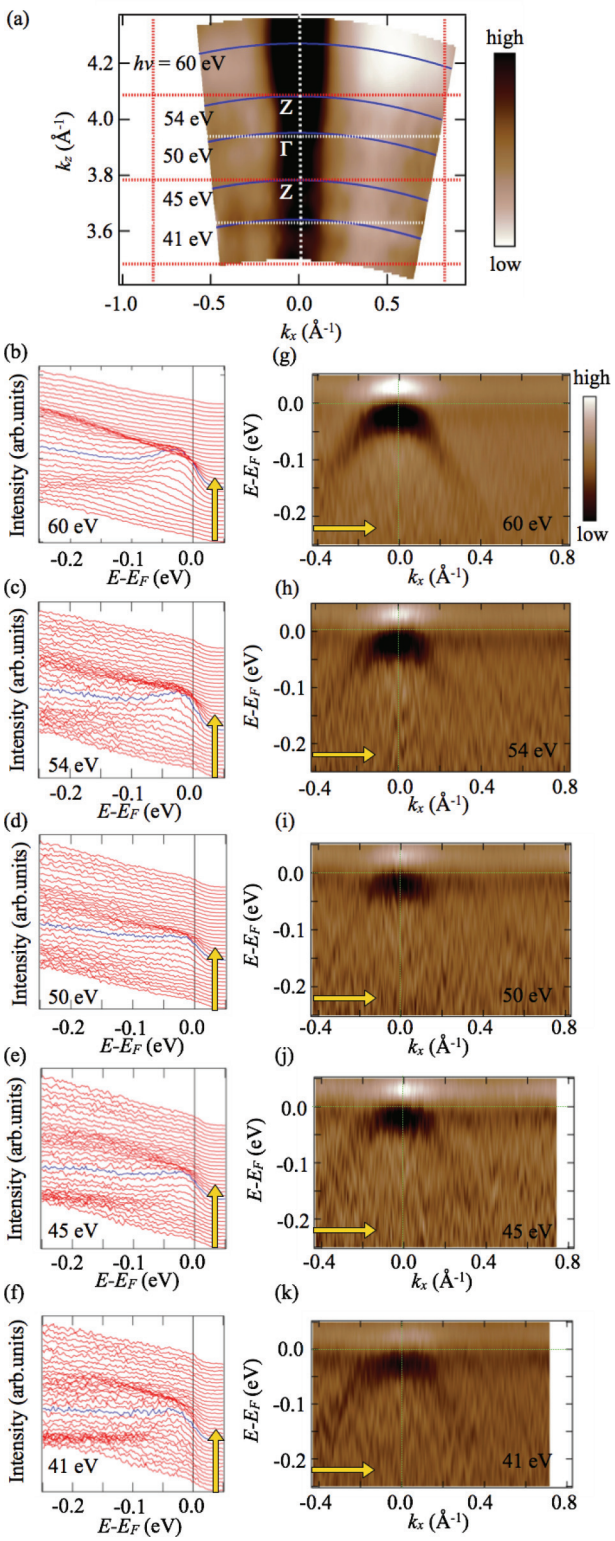

FIG. 3. (Color online) (a) Fermi surface map in the k_x-k_z plane taken at $h\nu = 37$–63 eV. k_x is the momentum approximately along the Fe-Fe direction of the FeAs layer. k_z is the momentum perpendicular to the FeAs layer. Energy distribution curves (b) at $h\nu = 60$ eV, (c) at $h\nu = 54$ eV, (d) at $h\nu = 50$ eV, (e) at $h\nu = 45$ eV, and (f) at $h\nu = 41$ eV. Second derivative plots (g) at $h\nu = 60$ eV, (h) at $h\nu = 54$ eV, (i) at $h\nu = 50$ eV, (j) at $h\nu = 45$ eV, and (k) at $h\nu = 41$ eV.

calculations. At the zone center, the As $4p_z$ orbitals of the FeAs layer hybridize with the Fe $3d\ xy$ orbital and the Ir $5d\ 3z^2 - r^2$ orbital in the neighboring Ir_4As_8 layer. Here, one can speculate that the Fe $3d\ xy$ orbital is strongly affected by the orbital instability between the Ir $5d\ 3z^2 - r^2$ and xy orbitals in the Ir_4As_8 layer [16] and is substantially broadened due to the Ir atomic (and orbital) disorder. On the other hand, the Fe $3d\ yz/zx$ orbitals are less affected by the Ir_4As_8 layer and are observed by ARPES. This assignment is further supported by the fact that the dispersion of the observed hole band agrees well with that of the Fe $3d\ yz/zx$ hole band reported in various systems.

In conclusion, we have studied the electronic structure of $Ca_{10}(Ir_4As_8)(Fe_{2-x}Ir_xAs_2)_5$ in which the metallic Ir_4As_8 layer with orbital degrees of freedom is expected to play important roles. The ARPES results indicate that the Ir $5d$ electrons are metallic and glassy probably due to atomic disorder related to the Ir $5d$ orbital instability [16]. On the other hand, the Fe $3d$ electrons in the FeAs layer form the holelike Fermi pocket at the zone center and the electronlike Fermi pockets at the zone corners as commonly seen in various Fe-based superconductors. While the hole band with the Fe $3d\ yz/zx$ character is clearly observed, other hole bands are smeared out probably due to the strong out-of-plane disorder from the Ir_4As_8 layer. The ARPES results indicate that the FeAs layer is heavily electron doped and has good two dimensionality. $Ca_{10}(Ir_4As_8)(Fe_{2-x}Ir_xAs_2)_5$ is characterized by the coexistence of the Bloch electrons in the FeAs layer and the glassy electrons in the Ir_4As_8 layer at E_F.

The authors would like to thank Dr. N. Katayama and Professor H. Sawa for valuable discussions and Professor T. Yokoya for information on $Ca_{10}(Pt_4As_8)(Fe_{2-x}Pt_xAs_2)_5$ prior to publication. This work was partially supported by Grants-in-Aid from the Japan Society of the Promotion of Science (JSPS) (Grants No. 22540363, No. 25400372, No. 25400356, and No. 26287082) and the Funding Program for World-Leading Innovative R&D on Science and Technology (FIRST Program) from JSPS. The synchrotron radiation experiment was performed with the approval of Photon Factory, KEK (Proposal No. 2013G021).

[1] Y. Kamihara, H. Hiramatsu, M. Hirano, R. Kawamura, H. Yanagi, T. Kamiya, and H. Hosono, J. Am. Chem. Soc. **128**, 10012 (2006).

[2] Y. Kamihara, T. Watanabe, M. Hirano, and H. Hosono, J. Am. Chem. Soc. **130**, 3296 (2008).

[3] H. Ding, P. Richard, K. Nakayama, K. Sugawara, T. Arakane, Y. Sekiba, A. Takayama, S. Souma, T. Sato, T. Takahashi, Z. Wang, X. Dai, Z. Fang, G. F. Chen, J. L. Luo, and N. L. Wang, Europhys. Lett. **83**, 47001 (2008).

[4] C. Liu, G. D. Samolyuk, Y. Lee, N. Ni, T. Kondo, A. F. Santander-Syro, S. L. Budko, J. L. McChesney, E. Rotenberg, T. Valla, A. V. Fedorov, P. C. Canfield, B. N. Harmon, and A. Kaminski, Phys. Rev. Lett. **101**, 177005 (2008).

[5] V. B. Zabolotnyy, D. S. Inosov, D. V. Evtushinsky, A. Koitzsch, A. A. Kordyuk, G. L. Sun, J. T. Park, D. Haug, V. Hinkov, A. V. Boris, C. T. Lin, M. Knupfer, A. N. Yaresko, B. Büchner, A. Varykhalov, R. Follath, and S. V. Borisenko, Nature (London) **457**, 569 (2009).

[6] Y. Zhang, J. Wei, H. W. Ou, J. F. Zhao, B. Zhou, F. Chen, M. Xu, C. He, G. Wu, H. Chen, M. Arita, K. Shimada, H. Namatame, M. Taniguchi, X. H. Chen, and D. L. Feng, Phys. Rev. Lett. **102**, 127003 (2009).

[7] K. Terashima, Y. Sekiba, J. H. Bowen, K. Nakayama, T. Kawahara, T. Sato, P. Richard, Y.-M. Xu, L. J. Li, G. H. Cao, Z.-A. Xu, H. Ding, and T. Takahashi, Proc. Natl. Acad. Sci. USA **106**, 7330 (2009).

[8] S. Kakiya, K. Kudo, Y. Nishikubo, K. Oku, E. Nishibori, H. Sawa, T. Yamamoto, T. Nozaka, and M. Nohara, J. Phys. Soc. Jpn. **80**, 093704 (2011).

[9] N. Ni, J. M. Allred, B. C. Chan, and R. J. Cava, Proc. Natl. Acad. Sci. **108**, E1019 (2011).

[10] C. Löhnert, T. Stürzer, M. Tegel, R. Frankovsky, G. Friederichs, and D. Johrendt, Angew. Chem., Int. Ed. **50**, 9195 (2011).

[11] M. Nohara, S. Kakiya, K. Kudo, Y. Oshiro, S. Araki, T. C. Kobayashi, K. Oku, E. Nishibori, and H. Sawa, Solid State Commun. **152**, 635 (2012).

[12] M. Neupane, C. Liu, S. Y. Xu, Y. J. Wang, N. Ni, J. M. Allred, L. A. Wray, N. Alidoust, H. Lin, R. S. Markiewicz, A. Bansil, R. J. Cava, and M. Z. Hasan, Phys. Rev. B **85**, 094510 (2012).

[13] S. Thirupathaiah, T. Stürzer, V. B. Zabolotnyy, D. Johrendt, B. Büchner, and S. V. Borisenko, Phys. Rev. B **88**, 140505 (2013).

[14] X. P. Shen, S. D. Chen, Q. Q. Ge, Z. R. Ye, F. Chen, H. C. Xu, S. Y. Tan, X. H. Niu, Q. Fan, B. P. Xie, and D. L. Feng, Phys. Rev. B **88**, 115124 (2013).

[15] K. Kudo, D. Mitsuoka, M. Takasuga, Y. Sugiyama, K. Sugawara, N. Katayama, H. Sawa, H. S. Kubo, K. Takamori, M. Ichioka, T. Fujii, T. Mizokawa, and M. Nohara, Sci. Rep. **3**, 3101 (2013).

[16] K. Sugawara, N. Katayama, Y. Sugiyama, T. Higuchi, K. Kudo, D. Mitsuoka, M. Nohara, and H. Sawa, arXiv:1402.3889.

[17] W. Malaeb, T. Yoshida, T. Kataoka, A. Fujimori, M. Kubota, K. Ono, H. Usui, K. Kuroki, R. Arita, H. Aoki, Y. Kamihara, M. Hirano, and H. Hosono, J. Phys. Soc. Jpn. **77**, 093714 (2008).

[18] T. Sudayama, Y. Wakisaka, T. Mizokawa, S. Ibuka, R. Morinaga, T. J. Sato, M. Arita, H. Namatame, M. Taniguchi, and N. L. Saini, J. Phys. Soc. Jpn. **80**, 113707 (2011).

[19] E. Paris, B. Joseph, A. Iadecola, C. Marini, K. Kudo, M. Nohara, T. Mizokawa, and N. L. Saini (unpublished).

[20] M. Sunagawa, R. Yoshida, T. Ishiga, K. Tsubota, T. Jabuchi, J. Sonoyama, S. Kakiya, D. Mitsuoka, K. Kudo, M. Nohara, K. Ono, H. Kumigashira, T. Oguchi, H. Iwasawa, K. Shimada, H. Namatame, M. Taniguchi, T. Wakita, Y. Muraoka, and T. Yokoya (unpublished).